J Sci Comput (2013) 55:432–454
DOI 10.1007/s10915-012-9640-5

A Finite Element Recovery Approach to Eigenvalue Approximations with Applications to Electronic Structure Calculations

Jun Fang · Xingyu Gao · Aihui Zhou

Received: 13 October 2011 / Revised: 21 May 2012 / Accepted: 28 August 2012 /
Published online: 8 September 2012

Abstract In this paper, we propose and analyze a recovery approach for trilinear finite element approximations on locally-refined hexahedral meshes for a class of elliptic eigenvalue problems. In the approach a local high-order interpolation recovery is followed by some gradient averaging based defect correction scheme. It is proved theoretically and shown numerically that our recovery approach can produce highly accurate eigenpair approximations. And we observe from our numerical experiments that the recovered eigenvalue approximation from the gradient averaging based defect correction approximates the exact eigenvalue from below. Furthermore, this approach has been applied to electronic structure calculations to improve the total energy approximations with small extra overheads.

Keywords Eigenpair recovery · Hexahedral finite element · Hanging node · Kohn–Sham equation · Gradient averaging · Lower bound

This work was partially supported by the National Science Foundation of China under grants 10871198, 10971059 and 61033009, the Funds for Creative Research Groups of China under grant 11021101, the National Basic Research Program of China under grants 2011CB309702 and 2011CB309703, and the National High Technology Research and Development Program of China under grant 2010AA012303.

J. Fang · A. Zhou (✉)
LSEC, Institute of Computational Mathematics and Scientific/Engineering Computing, Academy of Mathematics and Systems Science, Chinese Academy of Sciences, Beijing 100190, China
e-mail: azhou@lsec.cc.ac.cn

J. Fang
e-mail: fangjun@lsec.cc.ac.cn

J. Fang
Graduate University of Chinese Academy of Sciences, Beijing 100190, China

X. Gao
HPCC, Institute of Applied Physics and Computational Mathematics, Beijing 100094, China
e-mail: gao_xingyu@iapcm.ac.cn

1 Introduction

Eigenvalue problems are typical mathematical models in science and engineering. For instance, the Kohn–Sham equation, which is a nonlinear eigenvalue problem, plays an important role in modern electronic structure study [3, 17, 18, 20, 27]. We see that the numerical solving of eigenvalue problems is becoming increasingly important. In applications, efficient numerical methods to produce highly accurate approximations with lower computational cost are usually in demand. The finite element (FE) recovery technique is among one of them, and has been extensively studied in literature (see, e.g., [11, 12, 15, 23, 25, 29, 36] and references cited therein).

Motivated by the fact that for atomic and molecular systems, eigenfunctions of the Kohn–Sham equation have good regularity and only have large oscillations in the system region [3, 17], we develop in this paper a new recovery approach for the class of eigenvalue problems that eigenfunctions are smooth and vibrate rapidly in local regions. Most recently, we have proposed an interpolation based local recovery method in [13] to deal with the local vibrations. Note that the gradients of the interpolated eigenfunctions are still discontinuous, we further apply a gradient averaging approach, so as to compensate the regularity of the approximated solutions. Then we refine the eigenvalue approximations by a defect correction scheme [36]. Accordingly our recovery approach combines a local high-order interpolation with a gradient averaging based defect correction. The recovery approach does not need any auxiliary data and only requires small extra work. And the recovery at one point only involves its neighbors, which is distinguished from global projection operators used in many existing approaches.

For the sake of better accuracy and efficiency on a parallelepiped domain [9], we are particularly interested in hexahedral FE methods. We will study superconvergence of the recovery approach. Although the local interpolation recovery and the defect correction scheme have been analyzed in [13, 36], the analysis of their combination is beyond the extension of existing works. On the one hand, superconvergence result can not be easily obtained for eigenvalue approximations if using the local interpolation recovery alone [13]. On the other hand, unlike [36], we shall pay special attention to hanging nodes on our locally-refined hexahedral meshes. In addition, it should be mentioned that, the weights for gradient averaging are not specified in [36]. In the context of hexahedral FEs, we find that the harmonic averaging should be taken so as to yield an accurate local recovery.

Quite interestingly, we observe in our numerical experiments that the eigenvalue approximations from the gradient averaging based defect correction always approximate the exact eigenvalue from below. Note that all the conforming FE eigenvalue approximations are only upper bounds, it is significant to find the lower bound. Indeed, people have done a lot of work to get eigenvalue approximations from below. We refer to [19] by using mass-lumping FEs and others like [4, 23, 26, 35, 41, 45, 47, 49] by non-conforming FEs. As for our recovery approach, it could be viewed as some weighted averaging of the lower approximation from gradient averaging based defect correction and the upper one from interpolation recovery. It should be mentioned that currently we are not able to give a theoretical analysis for the observation.

The rest of this paper is organized as follows. In the next section, we introduce the notation, the FE discretization, and the definitions of interpolation and gradient averaging operators. We analyze superconvergence for eigenpair approximations of a model eigenvalue problem in Sect. 3. In Sect. 4, we illustrate several numerical experiments, not only to validate the theoretical results but also to illustrate some interesting phenomena. And then we apply the recovery approach particularly to Kohn–Sham equation in Sect. 5, which shows the effective enhancement of total energy approximations. Finally, we give some conclusions.

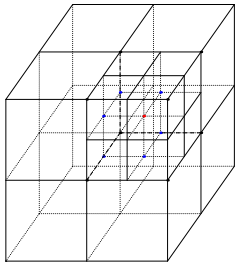

Fig. 1 Sketch for hanging nodes (*blue points* are hanging nodes) (Color figure online)

2 Preliminaries

In this section, we shall introduce notation and the FE discretization, and define the high-order interpolation and gradient averaging operators to be used in our recovery approach.

2.1 Notation

We shall use the standard notation for Sobolev space $W^{s,p}(\Omega)$ and their associated norms and seminorms; see, e.g., [2]. For $p = 2$, we denote $H^s(\Omega) = W^{s,2}(\Omega)$, $H_0^1(\Omega) = \{v \in H^1(\Omega) : v|_{\partial\Omega} = 0\}$, where $v|_{\partial\Omega} = 0$ is in the sense of trace, and $\|\cdot\|_{s,\Omega} = \|\cdot\|_{s,2,\Omega}$. In some places in this paper, $\|\cdot\|_{s,\Omega}$ should be viewed as piecewise defined if necessary. Throughout this paper, we use the notation $\lesssim$ other than $\leq$ to omit the positive constant.

In this paper we suppose $\Omega = (a_1, b_1) \times (a_2, b_2) \times (a_3, b_3)$ with $a_i, b_i \in \mathbb{R}$, $i = 1, 2, 3$. Our discretization will be performed on a locally-refined hexahedral mesh $T_h(\Omega)$ that consists of hexahedrons (cells) whose edges parallel to x-axis, y-axis and z-axis respectively, where h is the mesh size. It may be noticed that hanging nodes arise from the locally-refined hexahedral mesh. Hanging nodes occur on the shared face between one refined cell and an unrefined one, as illustrated in Fig. 1. In the following we denote by $\partial^3 T_h$ the set of all vertices of hexahedrons and by $\partial^3_{\mathrm{HN}} T_h$ the set of all the hanging nodes. Note that $\partial^3_{\mathrm{HN}} T_h \cap \partial\Omega = \varnothing$.

Define

$$S^{h,r}(\Omega) = \left\{v \in H^1(\Omega) : v|_\tau \in Q^r(\tau)\ \forall \tau \in T_h(\Omega)\right\},$$

$$S_0^{h,r}(\Omega) = S^{h,r}(\Omega) \cap H_0^1(\Omega),$$

where $Q^r(\tau) = \mathrm{span}\{x^i y^j z^k : 0 \leq i, j, k \leq r\}$ and $r = 1, 2$. In this paper, we write $S^h(\Omega)$ and $S_0^h(\Omega)$ representing $S^{h,1}(\Omega)$ and $S_0^{h,1}(\Omega)$ respectively. Let $I_h : C(\bar{\Omega}) \longrightarrow S^h(\Omega)$ be the trilinear Lagrange FE interpolation operator associated with $T_h(\Omega)$, namely, for $w \in C(\bar{\Omega})$

$$I_h w(p) = w(p) \quad \forall p \in \partial^3 T_h \setminus \partial^3_{\mathrm{HN}} T_h.$$

We shall study a finite element recovery approach to the following linear eigenvalue problem:

$$\begin{cases} -\nabla \cdot (A\nabla u) + \beta u = \lambda u, & \text{in } \Omega, \\ u = 0, & \text{on } \partial\Omega, \end{cases} \tag{1}$$

where A is a smooth positive definite symmetric matrix and $\beta \in L^\infty(\Omega)$.

Note that by a standard argument (see, e.g., [15, 25, 44]) we have

(i) If $T_h(\Omega)$ is without hanging nodes, then

$$\left|\int_\Omega A\nabla(w-I_hw)\cdot\nabla v\right| \lesssim h^{3/2}|w|_{5/2,\Omega}|v|_{1,\Omega} \quad \forall v\in S_0^h(\Omega) \tag{2}$$

when $w\in H_0^1(\Omega)\cap H^{5/2}(\Omega)$.

(ii) If $|\partial^3_{\mathrm{HN}}T_h| = \mathcal{O}(h^{-2})$, then

$$\left|\int_\Omega A\nabla(w-I_hw)\cdot\nabla v\right| \lesssim h^{3/2}\big(|w|_{5/2,\Omega}+|w|_{2,\infty,\Omega}\big)|v|_{1,\Omega} \quad \forall v\in S_0^h(\Omega) \tag{3}$$

when $w\in H_0^1(\Omega)\cap H^{5/2}(\Omega)\cap W^{2,\infty}(\Omega)$.

Hence we may assume in our analysis that if $w\in H_0^1(\Omega)\cap W^{5/2,\infty}(\Omega)$, then

$$\left|\int_\Omega A\nabla(w-I_hw)\cdot\nabla v\right| \lesssim h^{1+\theta}|w|_{5/2,\infty,\Omega}|v|_{1,\Omega} \quad \forall v\in S_0^h(\Omega), \tag{4}$$

where $\theta\in(0,1/2]$.

2.2 FE Discretization

The weak form of (1) is: Find $(\lambda,u)\in\mathbb{R}\times H_0^1(\Omega)$ such that

$$a(u,v)=\lambda(u,v) \quad \forall v\in H_0^1(\Omega), \tag{5}$$

where

$$a(w,v)=\int_\Omega (A\nabla w\cdot\nabla v+\beta wv) \quad \forall w,v\in H_0^1(\Omega).$$

The following property will be used in our analysis (see, e.g., [5, 6, 43]).

Proposition 1 *If $(\lambda,u)\in\mathbb{R}\times H_0^1(\Omega)$ satisfies (5), then*

$$\frac{a(w,w)}{\|w\|^2_{0,\Omega}}-\lambda=\frac{a(w-u,w-u)}{\|w\|^2_{0,\Omega}}-\lambda\frac{\|w-u\|^2_{0,\Omega}}{\|w\|^2_{0,\Omega}} \quad \forall w\in H_0^1(\Omega)\setminus\{0\}. \tag{6}$$

The FE discretization for (5) reads: Find $(\lambda_h,u_h)\in\mathbb{R}\times S_0^h(\Omega)$ such that

$$a(u_h,v)=\lambda_h(u_h,v) \quad \forall v\in S_0^h(\Omega). \tag{7}$$

Let $P_h: H_0^1(\Omega)\longrightarrow S_0^h(\Omega)$ be the Galerkin projection operator defined by

$$a(w-P_hw,v)=0 \quad \forall v\in S_0^h(\Omega). \tag{8}$$

We obtain from (7) and (8) that

$$a(P_hu-u_h,v)=\lambda(u-u_h,v)+(\lambda-\lambda_h)(u_h,v) \quad \forall v\in S_0^h(\Omega),$$

which gives a super-close relation between P_hu and u_h as follows (cf., e.g., [43]):

$$\|P_hu-u_h\|_{1,\Omega}\lesssim h^2 \tag{9}$$

when $u\in H_0^1(\Omega)\cap H^2(\Omega)$.

Since (4) produces

$$\|P_h u - I_h u\|_{1,\Omega} \lesssim h^{1+\theta} \tag{10}$$

when $u \in H_0^1(\Omega) \cap W^{5/2,\infty}(\Omega)$, we conclude from (9) and (10) that

$$\|u_h - I_h u\|_{1,\Omega} \lesssim h^{1+\theta} \tag{11}$$

if $u \in H_0^1(\Omega) \cap W^{5/2,\infty}(\Omega)$.

2.3 Two Operators

For any father cell $\square$ consisting of eight children hexahedrons in $T_h(\Omega)$, we can utilize the FE expansion coefficients of trilinear FE eigenfunctions $u_h \in S_0^h(\Omega)$ distributed over the eight cells to carry out a triquadratic Lagrange interpolation (denoted by Π_{2h}). We see that Π_{2h} has the following properties (cf. [13, 23]):

$$\Pi_{2h} I_h = \Pi_{2h}, \tag{12}$$

$$\|\nabla \Pi_{2h} v\|_{0,\square} \lesssim \|\nabla v\|_{0,\square} \quad \forall v \in S^h(\Omega), \tag{13}$$

$$\|\Pi_{2h} w - w\|_{1,\square} \lesssim h^2 \|w\|_{3,\square}. \tag{14}$$

Beside the interpolation operator, we shall also employ a gradient averaging operator $\mathcal{C}_h$ to recover the gradients over locally-refined hexahedral meshes. This operator is based on the average gradient value at each vertex (cf., e.g., [36]). For this purpose, given any vertex $p = (x_p, y_p, z_p) \in \partial^3 T_h$, define

$$\Lambda_p = \cup\big\{\bar{\tau} : \tau \in T_h(\Omega),\, p \in \bar{\tau}\big\},$$

and

$$H_{p,x}^+ = \big\{k > 0 : (x_p + k, y_p, z_p) \in \partial^3 T_h \cap \Lambda_p\big\},$$
$$H_{p,x}^- = \big\{k > 0 : (x_p - k, y_p, z_p) \in \partial^3 T_h \cap \Lambda_p\big\}.$$

We see that $H_{p,x}^+ \cup H_{p,x}^- \neq \varnothing$. Note that either of the following will be true:

(i) $H_{p,x}^+ = \varnothing$ and $p \in \partial\Omega$;
(ii) $H_{p,x}^- = \varnothing$ and $p \in \partial\Omega$;
(iii) $H_{p,x}^+ = \varnothing$ and $p \in \partial_{\mathrm{HN}}^3 T_h$;
(iv) $H_{p,x}^- = \varnothing$ and $p \in \partial_{\mathrm{HN}}^3 T_h$;
(v) $H_{p,x}^+ \neq \varnothing$ and $H_{p,x}^- \neq \varnothing$.

We define

$$(\partial_x v)(p) = \begin{cases} \partial_x v(p-), & \text{if } H_{p,x}^+ = \varnothing \text{ and } p \in \partial\Omega, \\ \partial_x v(p+), & \text{if } H_{p,x}^- = \varnothing \text{ and } p \in \partial\Omega, \\ \frac{h_{p,x}^+}{h_{p,x}^+ + h_{p,x}^-} \partial_x v(p-) + \frac{h_{p,x}^-}{h_{p,x}^+ + h_{p,x}^-} \partial_x v(p+), & \text{otherwise}, \end{cases} \tag{15}$$

where

$$h_{p,x}^+ = \begin{cases} \max\{k > 0 : (x_p + k, y_p, z_p) \in \Lambda_p\}, & \text{if } H_{p,x}^+ = \varnothing \text{ and } p \in \partial_{\mathrm{HN}}^3 T_h, \\ \min H_{p,x}^+, & \text{if } H_{p,x}^- = \varnothing \text{ and } p \in \partial_{\mathrm{HN}}^3 T_h, \\ \min H_{p,x}^+, & \text{if } H_{p,x}^+ \neq \varnothing \text{ and } H_{p,x}^- \neq \varnothing, \end{cases} \tag{16}$$

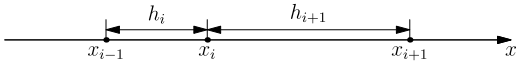

Fig. 2 One-dimensional sketch map for gradient averaging

$$h_{p,x}^{-}=\begin{cases}\min H_{p,x}^{-}, & \text{if } H_{p,x}^{+}=\varnothing \text{ and } p\in\partial_{\mathrm{HN}}^{3}T_h,\\ \max\{k>0:(x_p-k,y_p,z_p)\in\Lambda_p\}, & \text{if } H_{p,x}^{-}=\varnothing \text{ and } p\in\partial_{\mathrm{HN}}^{3}T_h,\\ \min H_{p,x}^{-}, & \text{if } H_{p,x}^{+}\neq\varnothing \text{ and } H_{p,x}^{-}\neq\varnothing.\end{cases}\tag{17}$$

With similar formulations, we define $(\partial_y v)(p)$ and $(\partial_z v)(p)$ and then obtain

$$(\nabla v)(p)=\big((\partial_x v)(p),(\partial_y v)(p),(\partial_z v)(p)\big)^{\mathsf{T}},$$

where superscript T represents the transpose. Now we construct the average gradient as follows:

$$\mathcal{C}_h A\nabla v=\sum_{p\in\partial^3 T_h}A(p)(\nabla v)(p)\phi_p,\tag{18}$$

where ϕ_p is the associated trilinear Lagrange basis function. We see that (cf., e.g., [36])

$$\|\mathcal{C}_h\nabla v\|_{0,G}\lesssim\|v\|_{1,G}\quad\forall v\in S^{h,r}(\Omega),\tag{19}$$

where domain $G\subset\Omega$ aligns with $T_h(\Omega)$.

Lemma 1 *If $u\in H_0^1(\Omega)\cap W^{5/2,\infty}(\Omega)$, then*

$$\big\|I_h(A\nabla u)-\mathcal{C}_h A\nabla(I_h u)\big\|_{0,\Omega}\lesssim h^{3/2}.\tag{20}$$

Proof We see from (18) that

$$\big\|I_h(A\nabla u)-\mathcal{C}_h A\nabla(I_h u)\big\|_{0,\Omega}\lesssim\max_{p\in\partial^3 T_h\setminus\partial\Omega}\big|\big(\nabla(I_h u)\big)(p)-\nabla u(p)\big|+h^{3/2}.$$

Thus we need to analyze $|(\nabla(I_h u))(p)-\nabla u(p)|$ for any vertex $p\in\partial^3 T_h\setminus\partial\Omega$. It is sufficient for us to estimate $(\partial_x(I_h u))(p)-\partial_x u(p)$ and consider a one-dimensional analysis as follows:

Let $a=x_0<x_1<\cdots<x_n=b$ be a partition of (a,b) and set $h_i=x_i-x_{i-1}$, $i=1,2,\ldots,n$. We analyze the average derivative of $I_h u$ on any point x_i (see Fig. 2). Denote by α the weight associated with $\partial_x(I_h u)(x_i-)$, then the average derivative can be written as

$$\begin{aligned}\big(\partial_x(I_h u)\big)(x_i)&=\alpha\frac{u(x_i)-u(x_{i-1})}{h_i}+(1-\alpha)\frac{u(x_{i+1})-u(x_i)}{h_{i+1}}\\&=\frac{1-\alpha}{h_{i+1}}u(x_{i+1})+\left(\frac{\alpha}{h_i}-\frac{1-\alpha}{h_{i+1}}\right)u(x_i)-\frac{\alpha}{h_i}u(x_{i-1}).\end{aligned}$$

Supposing u has the third derivative, we know from Taylor expansion that

$$\begin{aligned}\big(\partial_x(I_h u)\big)(x_i)-\partial_x u(x_i)&=\frac{(1-\alpha)h_{i+1}-\alpha h_i}{2}u^{(2)}(x_i)\\&\quad+\frac{(1-\alpha)h_{i+1}^2+\alpha h_i^2}{6}u^{(3)}(x_i)+\mathcal{O}\big(h^3\big).\end{aligned}$$

Set $\alpha = \frac{1}{h_i}/(\frac{1}{h_i} + \frac{1}{h_{i+1}})$ in the above expansion, we get

$$\max_{p\in\partial^3 T_h\setminus\partial\Omega} \left|\big(\partial_x(I_h u)\big)(p) - \partial_x u(p)\right| \lesssim h^2$$

when $u \in H_0^1(\Omega)\cap W^{3,\infty}(\Omega)$.

Finally, we complete the proof from Banach-space interpolation theory (cf. [10]) together with similar arguments for $(\partial_y(I_h u))(p) - \partial_y u(p)$ and $(\partial_z(I_h u))(p) - \partial_z u(p)$. □

We should mention that the harmonic averaging approach has been applied to obtain superconvergence over the rectangular mesh without hanging nodes in the literature (see, e.g., [46]).

3 The Recovery Approach

In this section, we will introduce and analyze the recovery approach to FE approximations for model problem (1). We shall employ both high-order interpolation operator and gradient averaging operator in our approach. The high-order interpolation is used in a local region indicated by an error indicator where eigenfunctions bear strong vibrations. And then the gradient averaging operator is performed globally in order to reconstruct a continuous gradient.

Given any eigenpair (λ_h, u_h) of (7) over a locally-refined hexahedral mesh, the recovery approach is carried out as follows:

1. Locate every father cell which has 8 children cells on the finest level in the hierarchy of the locally-refined mesh (all those father cells form the interpolation region denoted by Ω_0), and utilize the FE expansion coefficients of eigenfunction u_h distributed over the 8 children cells to carry out a triquadratic Lagrange interpolation Π_{2h} to obtain

$$\tilde{u}_h = \begin{cases} \Pi_{2h} u_h, & \text{in } \bar{\Omega}_0, \\ u_h, & \text{in } \Omega\setminus\bar{\Omega}_0. \end{cases} \tag{21}$$

2. Update the eigenvalue by Rayleigh quotient:

$$\tilde{\lambda}_h = \frac{\int_\Omega (|A^{1/2}\nabla\tilde{u}_h|^2 + \beta\tilde{u}_h^2)}{\|\tilde{u}_h\|_{0,\Omega}^2}. \tag{22}$$

3. Recover the gradient by $\mathcal{C}_h A\nabla\tilde{u}_h$.
4. Correct the eigenvalue by the defect correction:

$$\lambda_h^* = \tilde{\lambda}_h - \frac{\|A^{1/2}\nabla\tilde{u}_h - A^{-1/2}\mathcal{C}_h A\nabla\tilde{u}_h\|_{0,\Omega}^2}{\|\tilde{u}_h\|_{0,\Omega}^2}. \tag{23}$$

The following results can be derived (see, e.g., [24]).

Lemma 2

(i) *If* $u \in H_0^1(\Omega)\cap H^2(\Omega)$, *then*

$$\|u - \tilde{u}_h\|_{0,\Omega} + h|u - \tilde{u}_h|_{1,\Omega} \lesssim h^2. \tag{24}$$

(ii) *If* $u \in H_0^1(\Omega) \cap W^{2,\infty}(\Omega)$, *then*

$$|u - \tilde{u}_h|_{1,\infty,\Omega} \lesssim h. \tag{25}$$

(iii) *In the case of* $\Omega_0 = \Omega$ *and if* $u \in H_0^1(\Omega) \cap H^3(\Omega)$, *then*

$$|u - \tilde{u}_h|_{1,\Omega} \lesssim h^2. \tag{26}$$

We now study superconvergence for our eigenpair recovery approach. The superconvergence result for eigenvalue approximations is preceded by an estimation of the error in the recovered gradients of eigenfunctions. Better approximations of $A^{1/2}\nabla u$ are not only significant in their own right but also applied to improve eigenvalue approximations through defect correction.

Theorem 1 *If* $u \in H_0^1(\Omega) \cap W^{5/2,\infty}(\Omega)$, *then*

$$\left\| A^{1/2}\nabla u - A^{-1/2}\mathcal{C}_h A \nabla \tilde{u}_h \right\|_{0,\Omega} \lesssim h^{1+\theta}. \tag{27}$$

Proof We denote by Ω_1 the domain making up of all those cells in $T_h(\Omega)$ having some vertex on $\partial\Omega_0$, $D = \Omega_0 \setminus \bar{\Omega}_1$, and $\Omega_2 = \Omega \setminus (D \cup \bar{\Omega}_1)$.

From the definitions of $\tilde{u}_h$ and $\mathcal{C}_h$, we may divide $\|A^{1/2}\nabla u - A^{-1/2}\mathcal{C}_h A\nabla\tilde{u}_h\|_{0,\Omega}^2$ into three parts as follows:

$$\begin{aligned}\left\| A^{1/2}\nabla u - A^{-1/2}\mathcal{C}_h A \nabla \tilde{u}_h \right\|_{0,\Omega}^2 &= \left\| A^{1/2}\nabla u - A^{-1/2}\mathcal{C}_h A \nabla (\Pi_{2h} u_h) \right\|_{0,D}^2 \\ &\quad + \left\| A^{1/2}\nabla u - A^{-1/2}\mathcal{C}_h A \nabla u_h \right\|_{0,\Omega_2}^2 \\ &\quad + \left\| A^{1/2}\nabla u - A^{-1/2}\mathcal{C}_h A \nabla \tilde{u}_h \right\|_{0,\Omega_1}^2. \end{aligned} \tag{28}$$

Since (12) implies

$$\begin{aligned} A^{1/2}\nabla u - A^{-1/2}\mathcal{C}_h A \nabla (\Pi_{2h} u_h) &= A^{-1/2}\big(A\nabla u - I_h(A\nabla u)\big) \\ &\quad + A^{-1/2}\big(I_h(A\nabla u) - \mathcal{C}_h A \nabla (\Pi_{2h} u)\big) \\ &\quad + A^{-1/2}\mathcal{C}_h A \nabla \Pi_{2h}(I_h u - u_h), \end{aligned}$$

we get from the definitions of I_h and $\mathcal{C}_h$ that

$$\left\| A^{-1/2}\big(I_h(A\nabla u) - \mathcal{C}_h A \nabla (\Pi_{2h} u)\big) \right\|_{0,D} \lesssim |u - \Pi_{2h} u|_{1,\infty,D}.$$

While (13) and (19) lead to

$$\left\| A^{-1/2}\mathcal{C}_h A \nabla \Pi_{2h}(I_h u - u_h) \right\|_{0,D} \lesssim \left\| \Pi_{2h}(I_h u - u_h) \right\|_{1,D} \lesssim \|I_h u - u_h\|_{1,D}.$$

Thus we conclude that $\|A^{1/2}\nabla u - A^{-1/2}\mathcal{C}_h A\nabla(\Pi_{2h}u_h)\|_{0,D}$ can be bounded by

$$\left\| A\nabla u - I_h(A\nabla u) \right\|_{0,D} + |u - \Pi_{2h} u|_{1,\infty,D} + \|I_h u - u_h\|_{1,D}.$$

Noticing that there are no hanging nodes on domain $\bar{D}$, if $u \in H_0^1(\Omega) \cap W^{5/2,\infty}(\Omega)$, then

$$\left\| A^{1/2}\nabla u - A^{-1/2}\mathcal{C}_h A \nabla (\Pi_{2h} u_h) \right\|_{0,D} \lesssim h^{3/2}, \tag{29}$$

where (2) and (11) are used.

Similarly, since

$$\begin{aligned} A^{1/2}\nabla u - A^{-1/2}\mathcal{C}_h A\nabla u_h &= A^{-1/2}\big(A\nabla u - I_h(A\nabla u)\big) \\ &\quad + A^{-1/2}\big(I_h(A\nabla u) - \mathcal{C}_h A\nabla(I_h u)\big) \\ &\quad + A^{-1/2}\mathcal{C}_h A\nabla(I_h u - u_h), \end{aligned}$$

we can derive from (11), (19), and Lemma 1 that

$$\big\|A^{1/2}\nabla u - A^{-1/2}\mathcal{C}_h A\nabla u_h\big\|_{0,\Omega_2} \lesssim h^{1+\theta}. \tag{30}$$

For the last part in (28), since

$$A^{1/2}\nabla u - A^{-1/2}\mathcal{C}_h A\nabla\tilde{u}_h = A^{-1/2}\big(A\nabla u - I_h(A\nabla u)\big) + A^{-1/2}\big(I_h(A\nabla u) - \mathcal{C}_h A\nabla\tilde{u}_h\big),$$

we know from the definition of $\mathcal{C}_h$ that

$$\big\|A^{1/2}\nabla u - A^{-1/2}\mathcal{C}_h A\nabla\tilde{u}_h\big\|_{0,\Omega_1} \lesssim \big\|A\nabla u - I_h(A\nabla u)\big\|_{0,\Omega_1} + |u-\tilde{u}_h|_{1,\infty,\Omega_1}\cdot|\Omega_1|^{1/2}.$$

Notice that the measure of Ω_1 is in the order of $\mathcal{O}(h)$, thus we conclude from Lemma 2 that if $u\in H_0^1(\Omega)\cap W^{2,\infty}(\Omega)$, then

$$\big\|A^{1/2}\nabla u - A^{-1/2}\mathcal{C}_h A\nabla\tilde{u}_h\big\|_{0,\Omega_1} \lesssim h^{3/2} + h^{1/2}|u-\tilde{u}_h|_{1,\infty,\Omega} \lesssim h^{3/2}. \tag{31}$$

Combining (29), (30) and (31) we arrive at (27) when $u\in H_0^1(\Omega)\cap W^{5/2,\infty}(\Omega)$. This completes the proof. □

Now we turn to estimate the error in λ_h^*. Based on Proposition 1 and similar arguments as in [36], we have:

Lemma 3 *For any linear operator*

$$\mathcal{F}: S_0^h(\Omega)\longrightarrow H^1(\Omega)\times H^1(\Omega)\times H^1(\Omega),$$

there holds

$$\begin{aligned} \left|\frac{a(w,w)-\|A^{1/2}\nabla w-\mathcal{F}w\|_{0,\Omega}^2}{\|w\|_{0,\Omega}^2}-\lambda\right| &\lesssim \big\|A^{1/2}\nabla u-\mathcal{F}w\big\|_{0,\Omega}^2 \\ &\quad + \big\|A^{1/2}\nabla u-\mathcal{F}w\big\|_{0,\Omega}\cdot|w-u|_{1,\Omega} \\ &\quad + \|w-u\|_{0,\Omega}^2 \quad \forall w\in S_0^h(\Omega). \end{aligned} \tag{32}$$

Note that (32) has been shown in [36] when $w=u_h$, which can not be used directly in our analysis here, so we generalize it to any $w\in S_0^h(\Omega)$ as Lemma 3 stated.

Set $w=\tilde{u}_h$ and $\mathcal{F}=A^{-1/2}\mathcal{C}_h A\nabla$ in Lemma 3, we conclude the following result from Lemma 2 and Theorem 1:

Theorem 2 *If $u\in H_0^1(\Omega)\cap W^{5/2,\infty}(\Omega)$, then*

$$\big|\lambda_h^*-\lambda\big| \lesssim h^{2+\theta}. \tag{33}$$

Remark 1 In practice, $|\partial^3_{\mathrm{HN}} T_h| = \mathcal{O}(h^{-2})$ generally holds true, thus we have

$$\left\| A^{1/2}\nabla u - A^{-1/2}\mathcal{C}_h A\nabla \tilde{u}_h \right\|_{0,\Omega} \lesssim h^{3/2}, \tag{34}$$

$$\left|\lambda_h^* - \lambda\right| \lesssim h^{5/2}. \tag{35}$$

We know that a suitable regularity requirement should be reasonable in theoretical analysis for higher accuracy approximations. We will see from the numerical experiments that the high regularity of the eigenfunction is not always necessary to derive approximations with superconvergence.

Remark 2 In the case of $\Omega_0 = \Omega$ and $u \in H_0^1(\Omega) \cap W^{3,\infty}(\Omega)$, we have

$$\left\| A^{1/2}\nabla u - A^{-1/2}\mathcal{C}_h A\nabla \tilde{u}_h \right\|_{0,\Omega} \lesssim h^2, \tag{36}$$

$$\left|\lambda_h^* - \lambda\right| \lesssim h^4. \tag{37}$$

However, the starting point of our recovery approach is to improve the approximation accuracy of the eigenfunctions by high-order interpolation in a local region Ω_0 where oscillation happens, and we shall usually have $\Omega_0 \subsetneq \Omega$. Indeed, the most interesting case is $\Omega_0 \subsetneq \Omega$.

Remark 3 It may be noticed that if $\Omega_0 = \varnothing$, then our recovery approach reduces to the global gradient averaging based defect correction scheme developed and analyzed in [29, 36]. The difference is that, [29] focused on the polynomial preserving recovery (PPR), while [36] discussed tetrahedral FEs without explicit eigenfunction regularity restrictions.

Moreover, it will be shown from numerical experiments that our eigenvalue approximation λ_h^* is better than that from the global gradient averaging based defect correction.

4 Numerical Experiments

In this section, we provide numerical results for several typical eigenvalue problems to validate our theory and also show some interesting properties of the recovery approach.

We should mention that all the numerical implementation in this paper is based on deal.II [7], a C++ program library targeted at the computational solution of PDEs using adaptive FEs. And subroutines in ARPACK are called to solve the algebraic eigenvalue problems.

In our tables and figures, we use η_h to denote the error in Theorem 1:

$$\eta_h = \left\| A^{1/2}\nabla u - A^{-1/2}\mathcal{C}_h A\nabla \tilde{u}_h \right\|_{0,\Omega}.$$

And

$$e_h = \lambda_h - \lambda,$$
$$\tilde{e}_h = \tilde{\lambda}_h - \lambda, \qquad e_h^* = \lambda_h^* - \lambda,$$

are the differences between eigenvalue approximations and the real eigenvalue λ, where λ_h is the trilinear FE approximation, $\tilde{\lambda}_h$ the intermediate approximation as shown in (22), and λ_h^* the final approximation in (23).

Beside $\tilde{\lambda}_h$ and λ_h^* which appear in our recovery approach, we shall discuss eigenvalue approximation by using the gradient averaging based defect correction alone. Denote

$$\bar{\lambda}_h = \lambda_h - \left\| A^{1/2}\nabla u_h - A^{-1/2}\mathcal{C}_h A\nabla u_h \right\|_{0,\Omega}^2, \tag{38}$$

and define

$$\bar{e}_h = \bar{\lambda}_h - \lambda.$$

4.1 Typical Eigenvalue Problems

First, we describe four typical eigenvalue problems, on which we shall carry out numerical experiments to test our recovery approach.

1. The Laplace problem on the unit cube:

$$\begin{cases} -\Delta u = \lambda u, & \text{in } \Omega = (0,1)^3, \\ u = 0, & \text{on } \partial\Omega. \end{cases} \tag{39}$$

   The eigenvalues are given as $\lambda_{k,m,n} = \pi^2(k^2+m^2+n^2)$ and the associated eigenfunctions are $u_{k,m,n} = \gamma \sin(k\pi(x-1))\sin(m\pi(y-1))\sin(n\pi(z-1))$ where $k, m, n = 1, 2, \ldots$ and γ represents some nonzero constant (here and hereafter).
2. A variable-coefficient model problem:

$$\begin{cases} -\sum_{i=1}^3 \frac{\partial}{\partial x_i}(x_i^2 \frac{\partial u}{\partial x_i}) = \lambda u, & \text{in } \Omega = (1,3)\times(1,2)\times(1,2), \\ u = 0, & \text{on } \partial\Omega. \end{cases} \tag{40}$$

   The first eigenvalue is $\lambda = \frac{3}{4} + (\frac{2}{\ln^2 2} + \frac{1}{\ln^2 3})\pi^2$ and the associated eigenfunction is $u = \gamma \prod_{i=1}^3 (x_i^{-1/2}\sin(\frac{\pi \ln x_i}{\ln \beta_i}))$ where $\beta_1 = 3,\ \beta_2 = \beta_3 = 2$.
3. The quantum harmonic oscillator which is a simple model in quantum mechanics:

$$-\frac{1}{2}\Delta u + \frac{1}{2}|x|^2 u = \lambda u, \quad \text{in } \mathbb{R}^3. \tag{41}$$

   The first three different eigenvalues are 1.5, 2.5 and 3.5 with multiplicity 1, 3 and 6, respectively. And the eigenfunction associated with the first eigenvalue is $u = \gamma e^{-|x|^2/2}$. Since the eigenfunctions decay exponentially, the computation can be done on a finite domain imposed with the zero boundary condition. In our calculations, we set $\Omega = (-5.0, 5.0)^3$.
4. The linear Schrödinger equation of hydrogen atom:

$$-\frac{1}{2}\Delta u - \frac{1}{|x|}u = \lambda u, \quad \text{in } \mathbb{R}^3. \tag{42}$$

   The first two different eigenvalues are -0.5 and -0.125 with multiplicity 1 and 4 respectively. Considering the complexity of the eigenfunctions, we will only give numerical results for eigenvalues. In our calculation, the computational domain is chosen as $\Omega = (-20.0, 20.0)^3$. And we handle the singular term in this way: for any given quadrature point x, check if $|x| < 10^{-8}$; if it is, then we set $\frac{1}{|x|} = \frac{1}{|x|+10^{-8}}$.

Table 1 Error and convergence rate of the first eigenpair approximation

EVP	#DoFs	η_h	R(η_h)	e_h	$\tilde{e}_h$	$\lvert e_h^*\rvert$	R($\lvert e_h^*\rvert$)
1	54851	7.8152e–3	–	1.4788e–2	6.0787e–5	1.4082e–5	–
	189257	3.6725e–3	1.83	6.6914e–3	1.3221e–5	6.1454e–6	2.01
	453825	2.1832e–3	1.78	3.7838e–3	4.6603e–6	2.7592e–6	2.75
	892341	1.4547e–3	1.80	2.4280e–3	2.1170e–6	1.4667e–6	2.80
	1548847	1.0504e–3	1.77	1.6883e–3	1.1403e–6	8.6277e–7	2.89
2	11719	5.3279e–2	–	1.2855e–1	3.1612e–3	6.8775e–4	–
	99741	1.7845e–2	1.53	3.2242e–2	4.5380e–4	2.4557e–5	4.67
	343227	9.5924e–3	1.51	1.4430e–2	1.5570e–4	6.1314e–6	3.37
	821440	6.1943e–3	1.50	8.1317e–3	7.7760e–5	1.6989e–6	4.41
	1613482	4.4109e–3	1.51	5.2090e–3	4.6255e–5	9.0338e–7	2.81
3	12187	3.7462e–2	–	6.3179e–3	8.6033e–4	7.0986e–5	–
	102763	1.1803e–2	1.63	1.5627e–3	1.4603e–4	2.3434e–5	1.56
	353399	5.7912e–3	1.73	6.8997e–4	5.4953e–5	7.3431e–6	2.82
	845697	3.6130e–3	1.62	3.8685e–4	2.8485e–5	3.3138e–6	2.74
	1661263	2.4588e–3	1.71	2.4701e–4	1.7231e–5	1.7156e–6	2.93
4	12271	–	–	1.6257e–2	9.7211e–3	4.7306e–3	–
	102934	–	–	5.6265e–3	1.7927e–3	7.4882e–4	2.60
	353843	–	–	2.7848e–3	5.9032e–4	2.4226e–4	2.74
	846325	–	–	1.6512e–3	2.5949e–4	1.0794e–4	2.78
	1662333	–	–	1.0902e–3	1.3513e–4	5.7742e–5	2.78

4.2 Superconvergence

In this subsection, we give convergence results of the recovered eigenpair approximations and show that the approximations can be enhanced to a large extent.

Results in Theorems 1 and 2 and Remarks 1 and 2 tell that the recovered gradient approximation of the eigenfunction converges at a rate between $\mathcal{O}(h^{1.5})$ and $\mathcal{O}(h^2)$, and the recovered eigenvalue approximation converges at a rate between $\mathcal{O}(h^{2.5})$ and $\mathcal{O}(h^4)$. To test these, we carry out numerical experiments on the four problems, when we choose the interpolation domain to satisfy $\Omega_0 \subsetneq \Omega$.

We give in Table 1 the errors in recovered eigenpairs, η_h and $|e_h^*|$, and corresponding convergence rates calculated from any two adjacent results. In the table, EVP is short for eigenvalue problem, #DoFs represents the number of free degrees of freedom, and R(ξ_h) stands for the convergence rate of error ξ_h. It is shown that the numerical convergence rate coincides with the theory.

To exhibit the effectiveness of our recovery approach, we also give as a comparison errors e_h and $\tilde{e}_h$. It can be seen from the difference between e_h and e_h^* that our approach has greatly enhanced the FE approximations. And $|e_h^*| < \tilde{e}_h$ manifests that the approximation accuracy has been further improved by the gradient averaging based defect correction.

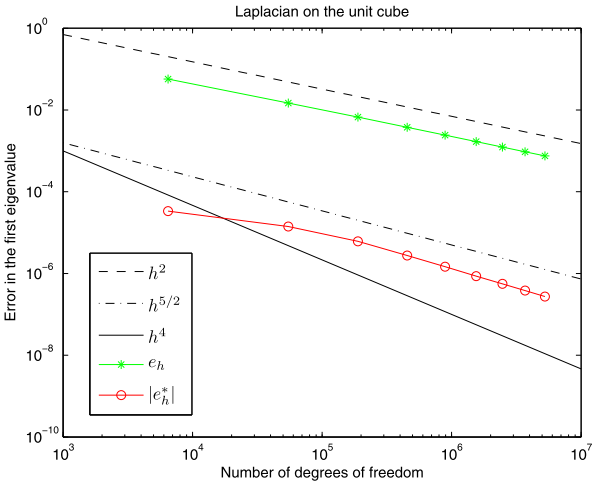

Fig. 3 Error in the first eigenvalue of Laplacian on the unit cube ($|\Omega_0| \approx 0.9|\Omega|$)

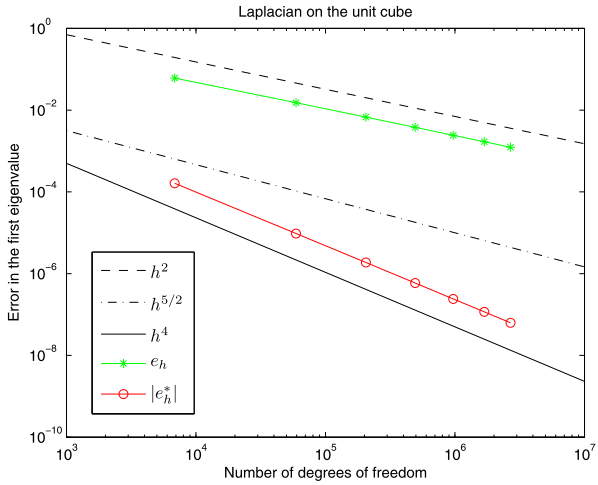

Fig. 4 Error in the first eigenvalue of Laplacian on the unit cube ($\Omega_0 = \Omega$)

4.3 Efficiency

In this subsection, we point out the class of eigenvalue problems on which our recovery approach would act most efficiently. Theoretical results in Sect. 3 read that the convergence rate of $|e_h^*|$ is between $\mathcal{O}(h^{2.5})$ and $\mathcal{O}(h^4)$, and a rate of $\mathcal{O}(h^4)$ can be reached when $\Omega_0 = \Omega$. However, the numerical experiments manifest that $\Omega_0 = \Omega$ is not always a necessary condition for rate $\mathcal{O}(h^4)$. The practical efficiency of the recovery approach is problem-dependent.

We choose to compare the results of the Laplacian on the unit cube and the quantum harmonic oscillator to illustrate the problem-dependence. For the former one, the convergence rate of $|e_h^*|$ under $|\Omega_0| \approx 0.9|\Omega|$ is nearly $\mathcal{O}(h^{2.5})$, and rate $\mathcal{O}(h^4)$ is reached when $\Omega_0 = \Omega$, as shown in Figs. 3 and 4. Unlike this, for quantum harmonic oscillator, as shown in Figs. 5 and 6, the convergence rate is improved to reach $\mathcal{O}(h^4)$ when Ω_0 is enlarged from $|\Omega_0| \approx 0.1|\Omega|$ to $|\Omega_0| \approx 0.2|\Omega|$.

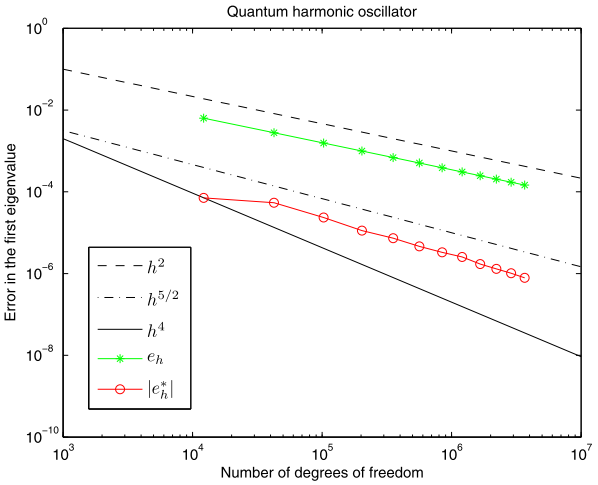

Fig. 5 Error in the first eigenvalue of harmonic oscillator ($|\Omega_0| \approx 0.1|\Omega|$)

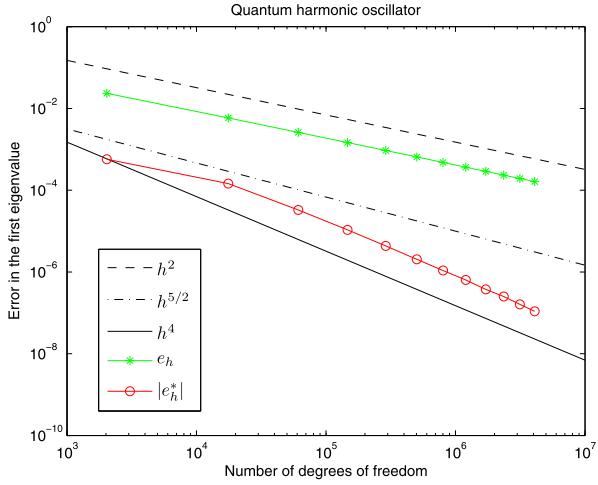

Fig. 6 Error in the first eigenvalue of harmonic oscillator ($|\Omega_0| \approx 0.2|\Omega|$)

The reason for this difference is distinct behaviors of the eigenfunctions. For oscillator, the region where the eigenfunction vibrates much is "local", and this region is located by our interpolation domain Ω_0. Therefore, the proposed recovery approach is more efficient for the class of problems of which the eigenfunction has local oscillations. And our approach is most approved to be applied to this kind of problems.

4.4 Approximation from Below

Beside the superconvergence and efficiency shown above, we observe from all our numerical experiments that $\bar{\lambda}_h$ defined by (38) approximates the exact eigenvalue from below, as shown by the dark blue lines with crosses in Fig. 7. In this sense, the gradient averaging based defect correction may probably provide a new way to find the lower bound for eigenvalues. Since all the conforming FE eigenvalue approximations are only upper bounds, it is significant to

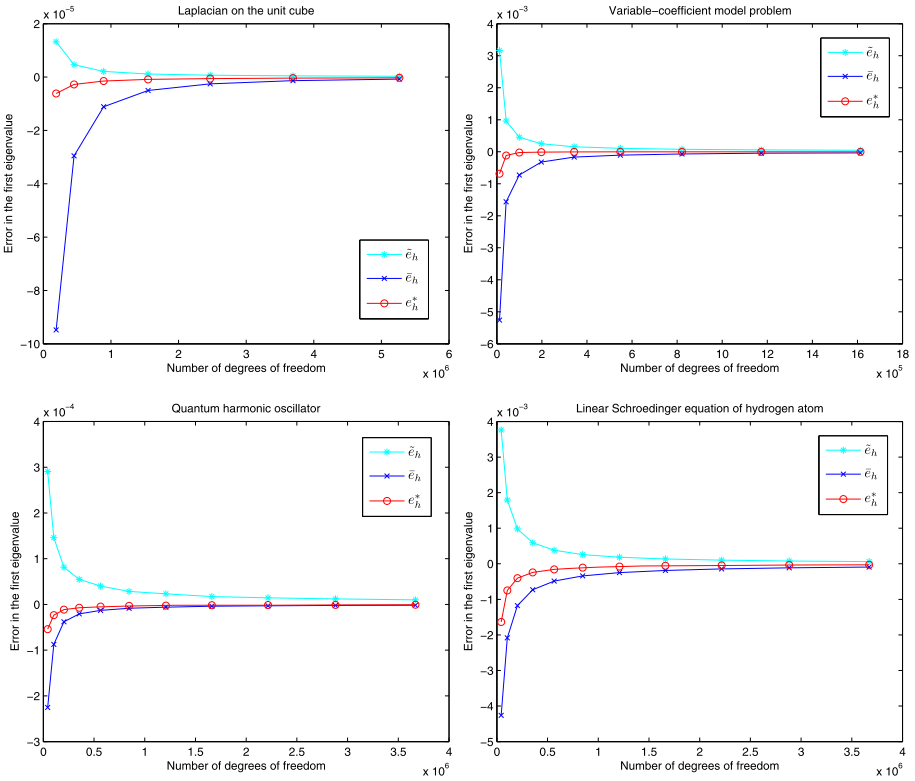

Fig. 7 Eigenvalue approximation properties of the recovery approaches (Color figure online)

find the lower bound. Indeed many efforts have been made to get eigenvalue approximation from below. We refer to [19] by using mass-lumping FEs, and others like [4, 23, 26, 35, 41, 45, 47, 49] by non-conforming FEs. Note that the gradient averaging based defect correction is carried out on conforming FEs.

As the approximation from interpolation recovery approximates the exact eigenvalue from above, our recovery approach may be viewed as some weighted averaging of interpolation recovery and the gradient averaging based defect correlation. By weighted we mean that our recovery approach is not just a simple averaging of those two techniques, but exhibits some selection between the two, as shown in Fig. 7. In the figure, our recovery approach, the interpolation recovery, and the gradient averaging based defect correction correspond to the red lines with circles, the light blue lines with asterisks, and the dark blue lines with crosses, respectively.

Currently we are not able to give a theoretical support for the observation. It is still open whether a rigorous analysis is possible. It should be mentioned that the numerical experiments in [36] also imply that the eigenvalue approximation after gradient averaging based defect correlation (denoted by $\tilde{\lambda}_{h,G_h}$ there) approximates the exact eigenvalue from below. Specifically, for all the linear eigenvalue problems with smooth coefficients in [36], numerical results do indicate that $\tilde{\lambda}_{h,G_h}$ approximates the exact eigenvalue from below. However,

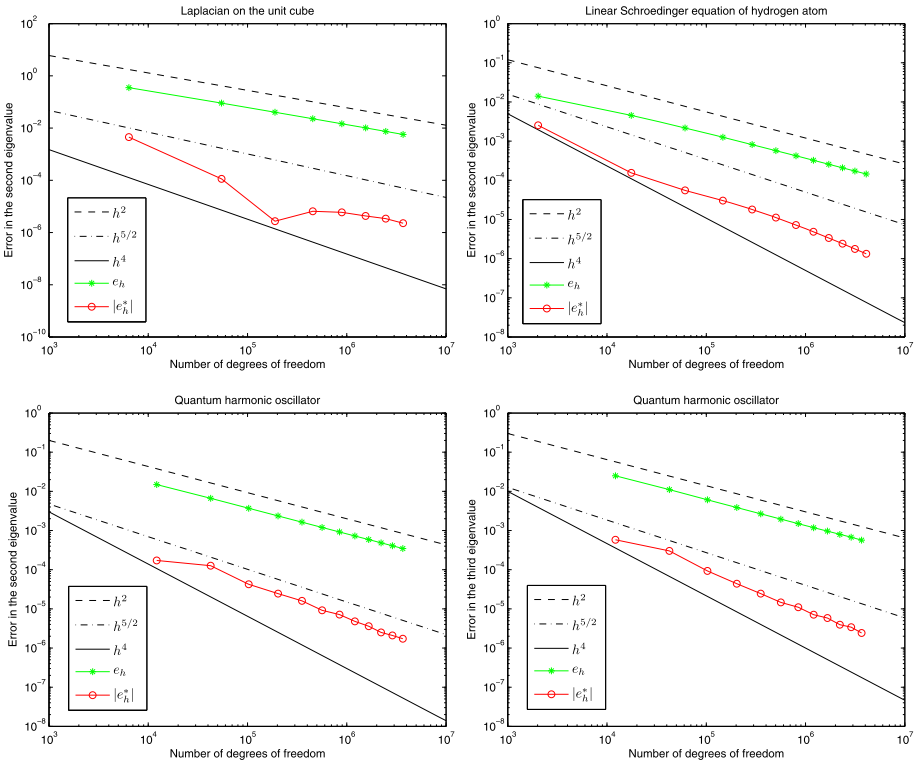

Fig. 8 Convergence rate of the eigenvalue approximations under multiplicity

for the linear Schrödinger equation of hydrogen atom, we find it difficult to observe this property if lack of the careful handling of singular term $\frac{1}{|x|}$.

4.5 Results for Multiple Eigenvalues

In the above subsections we only address the case of simple or non-degenerate eigenvalues. We would like to show in this subsection that similar conclusions have been obtained for multiple or degenerate eigenvalues.

We take the Laplacian on the unit cube, the quantum harmonic oscillator, and linear Schrödinger equation of hydrogen atom as the examples. For the Laplacian, we give results of the second eigenvalue, which has multiplicity 3. For the oscillator, we compute the second and the third eigenvalues with multiplicity 3 and 6 respectively. And for hydrogen atom the second eigenvalue which has multiplicity 4.

Figure 8 tells that the same convergence rate holds for the multiple eigenvalues. In Fig. 9, we can see that $\bar{\lambda}_h$ (approximation from the gradient averaging based defect correlation) approximates the exact eigenvalue from below, and the error in λ_h^* (approximation from our recovery approach) is between that of $\tilde{\lambda}_h$ (approximation from the local high-order interpolation recovery) and $\bar{\lambda}_h$.

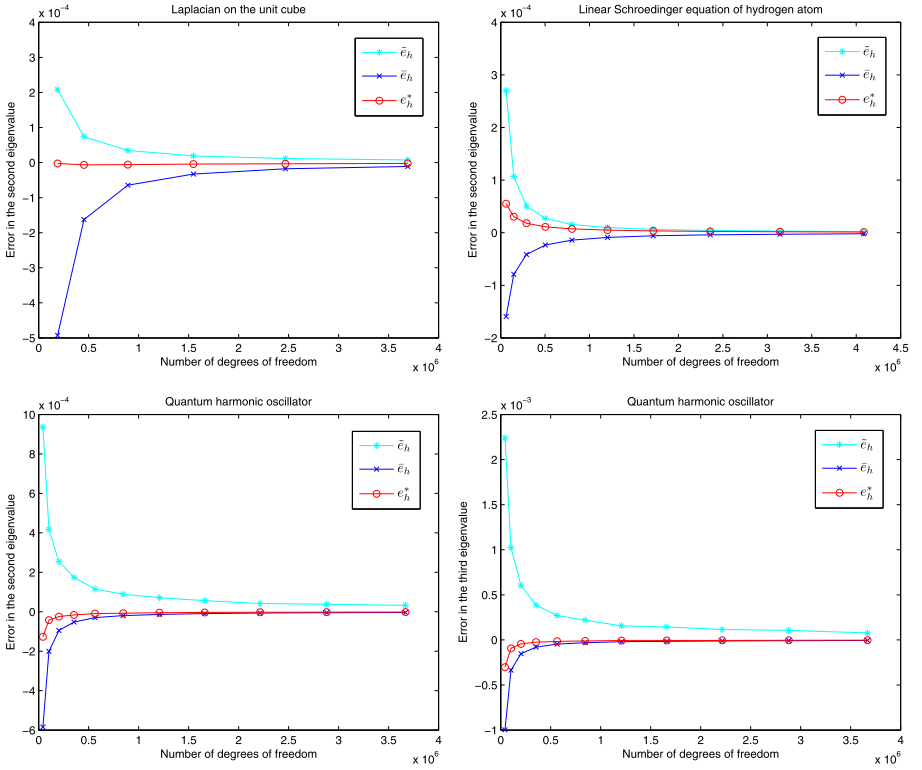

Fig. 9 Eigenvalue approximation properties of the recovery approaches under multiplicity

5 Applications to Total Energy Calculations

In this section, we apply the proposed recovery approach to enhance the eigenvalue approximations of the Kohn–Sham equation, which are then used to improve the total energy results of molecular systems.

Density Functional Theory (DFT) reveals the significance of the ground state density in electronic structure study [18]. In modern DFT calculations, the ground state properties are usually obtained by solving the Kohn–Sham equation [18, 20, 27]. Since the ground state density of a confined system decays exponentially [3, 16, 37], we may solve the associated Kohn–Sham equation posed on some appropriately cuboid domain $\Omega \subset \mathbb{R}^3$ as

$$\left(-\frac{1}{2}\Delta + V^{\text{eff}}[\rho]\right)\Psi_n = \epsilon_n \Psi_n, \quad \text{in } \Omega \tag{43}$$

with the zero boundary condition, where $\rho(\mathbf{r}) = \sum_{n=1}^{N_s} f_n |\Psi_n(\mathbf{r})|^2$ is the charge density contributed by N_s orbitals $\{\Psi_n\}$ with associated occupancy numbers $\{f_n\}$, and $V^{\text{eff}}[\rho]$ the so-called effective potential that is a nonlinear functional of ρ.

If without external fields, the effective potential in Kohn–Sham equation (43) can be written into three parts:

$$V^{\text{eff}} = V^{\text{ne}} + V^{\text{H}} + V^{\text{xc}}, \tag{44}$$

where V^{ne} is the Coulomb potential between the nuclei and the electrons, V^{H} the Hartree potential, and V^{xc} the exchange-correlation potential [27]. In our calculation, we use norm-conserving pseudopotentials to replace the strong Coulomb potential V^{ne}, the Hartree potential is obtained by solving the Poisson equation where boundary values are approximated by multipole expansion [22], and we compute the exchange-correlation potential using the local density approximation (LDA)

$$V^{\mathrm{xc}}[\rho] = \frac{\delta(\int_{\Omega} \rho(\mathbf{r})\epsilon^{\mathrm{xc}}[\rho(\mathbf{r})]d\mathbf{r})}{\delta\rho} \tag{45}$$

with a given parameterized functional ϵ^{xc} [32]. In this framework, the ground state total energy can be achieved as follows (cf. [27]):

$$E_{\mathrm{tot}} = \sum_{n=1}^{N_s} f_n\epsilon_n - \int_{\Omega} \rho(\mathbf{r})V^{\mathrm{xc}}\big[\rho(\mathbf{r})\big]d\mathbf{r} - \frac{1}{2}\int_{\Omega} \rho(\mathbf{r})V^{\mathrm{H}}\big[\rho(\mathbf{r})\big]d\mathbf{r} + \int_{\Omega} \rho(\mathbf{r})\epsilon^{\mathrm{xc}}\big[\rho(\mathbf{r})\big]d\mathbf{r} + \frac{1}{2}\sum_{I,J=1,I\neq J}^{N_{\mathrm{nuclei}}} \frac{Z_I Z_J}{|\mathbf{R}_I - \mathbf{R}_J|}, \tag{46}$$

where $\mathbf{R}_I$ and Z_I^{ion} represent the position and valence of the I-th atom, respectively.

Since Kohn–Sham equation (43) is a nonlinear eigenvalue problem, it needs to be solved by the self-consistent field (SCF) iteration [27]. The dominant part of computation is the repeated solution of the following linearized Kohn–Sham equation:

$$\left(-\frac{1}{2}\Delta + V^{\mathrm{eff}}[\rho_{\mathrm{in}}]\right)\Psi_n = \epsilon_n\Psi_n, \quad \text{in } \Omega, \tag{47}$$

where ρ_{in} is the input density at each iteration step.

The real-space discretization methods are attractive for the confined systems since they allow a natural imposition of the zero boundary condition [8, 21]. In real-space representations, the potential operator is diagonal and the Laplacian is nearly local. This locality is suited for massively parallel processing and is also the basis for the development of linear-scaling methods [8]. As one kind of real-space mesh techniques, FE methods keep the locality and the variational property at the same time, and have been applied to electronic structure calculations (see, e.g., [1, 13, 14, 30, 31, 38–40, 42, 48] and references cited therein).

In our computation, Kohn–Sham equation (43) is discretized by locally-refined hexahedral FEs. We construct the initial density ρ_0 by some combination of the pseudo atomic orbitals. Based on the initial density, we carry out local mesh refinements according to the following local error indicator:

$$h_\tau \|\nabla\rho_0\|_{0,\tau} \quad \forall\tau \in T_h(\Omega), \tag{48}$$

and then start the SCF iteration using trilinear FEs distributed over this mesh. In the SCF iteration, we mix densities using Pulay's method [33, 34].

When SCF convergence is reached, we utilize the proposed recovery approach to refine the FE approximations. And then update the band energy part $\sum_{n=1}^{N_s} f_n\epsilon_n$ in (46) to improve the total energy approximation (from $E_{\mathrm{tot},h}$ to $E^*_{\mathrm{tot},h}$). We simply update the band energy part, but have not computed a new density from the recovered wavefunctions to modify the

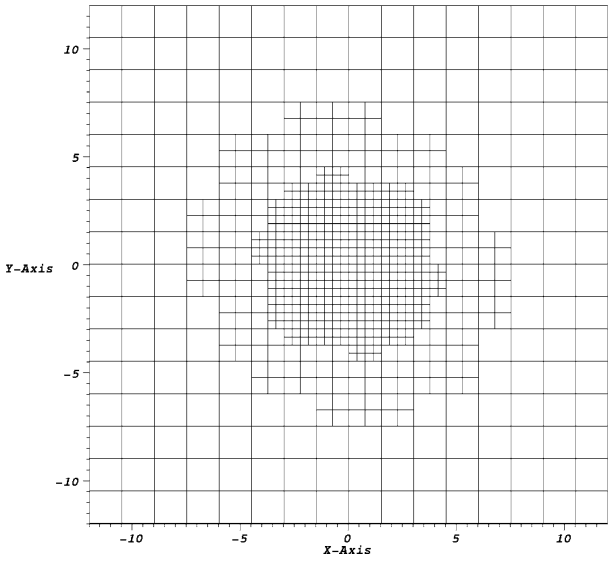

Fig. 10 Mesh for SiH_4 at $z = 0.0$ Å

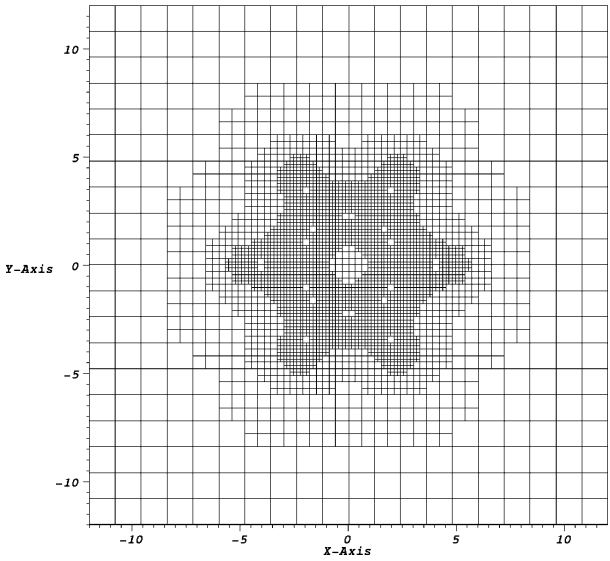

Fig. 11 Mesh for C_6H_6 at $z = 0.0$ Å

other parts. The reason is that the interpolation recovery will break the orthonormality of wavefunctions. According to our experience, it may induce incorrect modifications in the energy approximations if we renormalize the recovered eigenfunctions and then update the other parts in the total energy functional.

Here we calculate four systems as testing applications, including silane SiH_4, benzene C_6H_6, aspirin $C_9H_8O_4$, and fullerene C_{60}. The energy is measured in eV in this paper. The locally-refined hexahedral meshes are given in Figs. 10, 11, 12, and 13. We should mention that the locally-refined meshes are visualized by JaVis [28].

We give the errors of total energy per atom before and after recovery in Column 3 and Column 4 of Table 2, where the errors are estimated with respect to results from indepen-

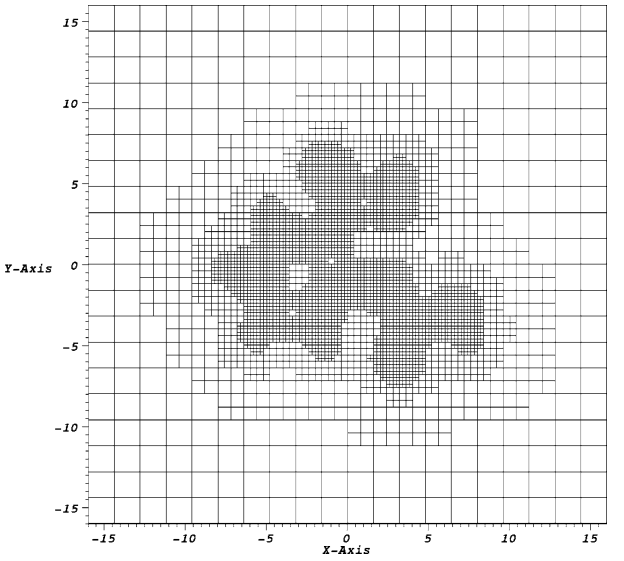

Fig. 12 Mesh for $C_9H_8O_4$ at $z = 0.0$ Å

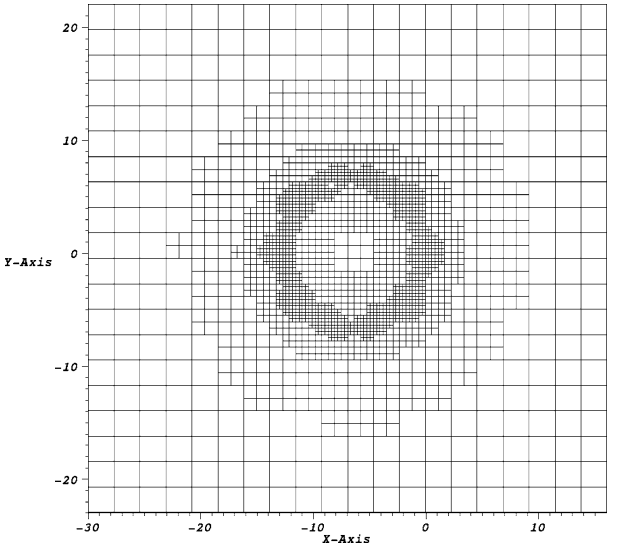

Fig. 13 Mesh for C_{60} at $z = 0.0$ Å

dent fully-converged plane wave calculations. To better illustrate the effectiveness, we also calculate the percentage of the time for recovery out of the total time. It can be seen that our recovery approach could enhance the total energy approximations with small extra overheads.

Note that the time percentage of recovery is decreasing with the size of the system. This is because the time spent on computing eigenvalue problems is increasing much faster. In the case of C_{60}, the percentage is sharply declined due to a much longer time for solving the algebraic eigenvalue problem, while the error is decreased by one magnitude. So it is indicated that developing appropriate recovery techniques would be attractive for larger systems.

Table 2 Total energy enhancement by the recovery approach

System	N_s	$E_{\text{tot},h}/N_{\text{nuclei}}$ err.	$E^*_{\text{tot},h}/N_{\text{nuclei}}$ err.	$\frac{\text{Recovery time}}{\text{Total time}}$
SiH_4	4	4.7102e–1	2.3891e–2	12.04 %
C_6H_6	15	4.8156e–1	1.1783e–2	9.48 %
$C_9H_8O_4$	34	1.6482e–0	1.0366e–1	9.14 %
C_{60}	120	3.6014e–0	4.0592e–1	1.43 %

6 Concluding Remarks

We have proposed and analyzed an eigenpair recovery approach to improve the FE approximations on locally-refined hexahedral meshes. We have demonstrated superconvergence for eigenpair approximations of a model eigenvalue problem. Our numerical experiments on several linear eigenvalue problems well supported the theory and reflected the more efficient cases to use this approach. Quite interestingly, we have observed from our numerical experiments that the recovered eigenvalue approximation from our gradient averaging based defect correlation approximates the exact eigenvalue from below, although we still lack rigorous theoretical analysis. Applications to Kohn–Sham equation exhibited reasonable enhancement in the total energy approximations. Some rigorous explanation of the approximation properties will be studied in the future work.

Acknowledgements The authors would like to thank Prof. Xiaoying Dai, Prof. Xingao Gong, Prof. Lihua Shen, and Dr. Zhang Yang for their stimulating discussions and fruitful cooperations on electronic structure computations. The second author is grateful to Prof. Zeyao Mo for his encouragements. The authors would also like to thank the referees for their constructive comments and suggestions that improve the presentation of this paper.

References

1. Ackermann, J., Erdmann, B., Roitzsch, R.: A self-adaptive multilevel finite element method for the stationary Schrödinger equation in three space dimensions. J. Chem. Phys. **101**, 7643–7650 (1994)
2. Adams, R.A.: Sobolev Spaces. Academic Press, New York (1975)
3. Agmon, S.: Lectures on the Exponential Decay of Solutions of Second-Order Elliptic Operators. Princeton University Press, Princeton (1981)
4. Armentano, M., Duran, R.: Asymptotic lower bounds for eigenvalues by nonconforming finite element methods. Electron. Trans. Numer. Anal. **17**, 92–101 (2004)
5. Babuska, I., Osborn, J.E.: Finite element-Galerkin approximation of the eigenvalues and eigenvectors of self-adjoint problems. Math. Comput. **52**(186), 275–297 (1989)
6. Babuska, I., Osborn, J.E.: Eigenvalue problems. In: Handbook of Numerical Analysis, vol. II, pp. 641–787. North-Holland, Amsterdam (1991)
7. Bangerth, W., Hartmann, R., Kanschat, G.: Deal. II—A general-purpose object-oriented finite element library. ACM Trans. Math. Softw. **33**, 24:1–24:27 (2007)
8. Beck, T.L.: Real-space mesh techniques in density-functional theory. Rev. Mod. Phys. **72**, 1041–1080 (2000)
9. Brauer, J.R.: What Every Engineer Should Know About Finite Element Analysis. Marcel Decker, New York (1993)
10. Brenner, S.C., Scott, L.R.: The Mathematical Theory of Finite Element Methods. Springer, New York (1994)
11. Dai, X., Zhou, A.: Three-scale finite element discretizations for quantum eigenvalue problems. SIAM J. Numer. Anal. **46**, 295–324 (2008)
12. Dai, X., Shen, L., Zhou, A.: A local computational scheme for higher order finite element eigenvalue approximations. Int. J. Numer. Anal. Model. **5**, 570–589 (2008)

13. Fang, J., Gao, X., Gong, X., Zhou, A.: Interpolation based local postprocessing for adaptive finite element approximations in electronic structure calculations. In: Huang, Y., Kornhuber, R., Widlund, O., Xu, J. (eds.) Domain Decomposition Methods in Science and Engineering XIX. Lecture Notes in Computational Science and Engineering, vol. 78, pp. 51–61. Springer, Berlin (2011)
14. Fattebert, J.-L., Hornung, R.D., Wissink, A.M.: Finite element approach for density functional theory calculations on locally-refined meshes. J. Comput. Phys. **223**, 759–773 (2007)
15. Gao, X., Liu, F., Zhou, A.: Three-scale finite element eigenvalue discretizations. BIT Numer. Math. **48**(3), 533–562 (2008)
16. Gilbarg, D., Trudinger, N.S.: Elliptic Partial Differential Equations of Second Order, 3rd edn. Springer, Berlin (2001)
17. Gong, X., Shen, L., Zhang, D., Zhou, A.: Finite element approximations for Schrödinger equations with applications to electronic structure computations. J. Comput. Math. **23**, 310–327 (2008)
18. Hohenberg, P., Kohn, W.: Inhomogeneous electron gas. Phys. Rev. B **136**(3), 864–871 (1964)
19. Hu, J., Huang, Y., Shen, H.: The lower approximation of eigenvalue by lumped mass finite element method. J. Comput. Math. **22**, 545–556 (2004)
20. Kohn, W., Sham, L.J.: Self-consistent equations including exchange and correlation effects. Phys. Rev. **140**(4A), A1133–A1138 (1965)
21. Kronik, L., Makmal, A., Tiago, M.L., Alemany, M.M.G., Jain, M., Huang, X., Saad, Y., Chelikowsky, J.R.: Parsec—the pseudopotential algorithm for real-space electronic structure calculations: recent advances and novel applications to nano-structures. Phys. Status Solidi (b) **243**, 1063–1079 (2006)
22. Landau, L.D., Lifshitz, E.M.: The Classical Theory of Fields. Pergamon Press, Oxford (1975)
23. Lin, Q., Lin, J.: Finite Element Methods: Accuracy and Improvement. Science Press, Beijing (2006)
24. Lin, Q., Yang, Y.: Interpolation and correction of finite elements. Math. Pract. Theory **3**, 29–35 (1991) (in Chinese)
25. Lin, Q., Zhu, Q.: The Preprocessing and Postprocessing for the Finite Element Method. Shanghai Scientific & Technical Publishers, Shanghai (1994) (in Chinese)
26. Liu, H., Yan, N.: Four finite element solutions and comparison of problem for the Poisson equation eigenvalue. Chin. J. Numer. Math. Comput. Appl. **2**, 81–91 (2005) (in Chinese)
27. Martin, R.M.: Electronic Structure: Basic Theory and Practical Methods. Cambridge University Press, Cambridge (2004)
28. Mo, Z., Zhang, A. (eds.): User's guide for JASMIN. Technical Report No. T09-JMJL-01 (2009). http://www.iapcm.ac.cn/jasmin
29. Naga, A., Zhang, Z., Zhou, A.: Enhancing eigenvalue approximation by gradient recovery. SIAM J. Sci. Comput. **28**, 1289–1300 (2006)
30. Pask, J.E., Klein, B.M., Fong, C.Y., Sterne, P.A.: Real-space local polynomial basis for solid-state electronic-structure calculations: A finite-element approach. Phys. Rev. B **59**, 12352–12358 (1999)
31. Pask, J.E., Sterne, P.A.: Finite element methods in ab initio electronic structure calculations. Model. Simul. Mater. Sci. Eng. **13**, 71–96 (2005)
32. Perdew, J.P., Zunger, A.: Self-interaction correction to density-functional approximations for many-electron systems. Phys. Rev. B **23**, 5048–5079 (1981)
33. Pulay, P.: Convergence acceleration of iterative sequences in the case of SCF iteration. Chem. Phys. Lett. **73**, 393–398 (1980)
34. Pulay, P.: Improved SCF convergence acceleration. J. Comput. Chem. **3**, 556–560 (1982)
35. Rannacher, R.: Nonconforming finite element methods for eigenvalue problems in linear plate theory. Numer. Math. **33**, 23–42 (1979)
36. Shen, L., Zhou, A.: A defect correction scheme for finite element eigenvalues with applications to quantum chemistry. SIAM J. Sci. Comput. **28**, 321–338 (2006)
37. Simon, B.: Schrödinger operators in the twentieth century. J. Math. Phys. **41**, 3523–3555 (2000)
38. Sterne, P.A., Pask, J.E., Klein, B.M.: Calculation of positron observables using a finite element-based approach. Appl. Surf. Sci. **149**, 238–243 (1999)
39. Suryanarayana, P., Gavini, V., Blesgen, T.: Non-periodic finite-element formulation of Kohn-Sham density functional theory. J. Mech. Phys. Solids **58**, 256–280 (2010)
40. Tsuchida, E., Tsukada, M.: Electronic-structure calculations based on the finite-element method. Phys. Rev. B **52**, 5573–5578 (1995)
41. Weinstein, A., Chien, W.: On the vibrations of a clamped plate under tension. Q. Appl. Math. **1**, 61–68 (1943)
42. White, S.R., Wilkins, J.W., Teter, M.P.: Finite-element method for electronic structure. Phys. Rev. B **39**, 5819–5833 (1989)
43. Xu, J., Zhou, A.: A two-grid discretization scheme for eigenvalue problems. Math. Comput. **70**, 17–25 (2001)

44. Yan, N.: Superconvergence Analysis and a Posteriori Error Estimation in Finite Element Methods. Science Press, Beijing (2008)
45. Yang, Y., Zhang, Z., Lin, F.: Eigenvalue approximation from below using non-conforming finite elements. Sci. China Ser. A **53**, 137–150 (2010)
46. Yi, N.: A posteriori error estimates based on gradient recovery and adaptive finite element methods. Ph.D. thesis, School of Mathematics and Computational Science, Xiangtan University, Xiangtan (2011)
47. Zhang, Z., Yang, Y., Chen, Z.: Eigenvalue approximation from below by Wilson's element. Chin. J. Numer. Math. Appl. **29**, 81–84 (2007)
48. Zhang, D., Shen, L., Zhou, A., Gong, X.: Finite element method for solving Kohn-Sham equations based on self-adaptive tetrahedral mesh. Phys. Lett. A **372**, 5071–5076 (2008)
49. Zienkiewicz, O., Cheung, Y.: The Finite Element Method in Structural and Continuum Mechanics. McGraw-Hill, New York (1967)